Unveiling the dual role of chemically synthesized copper doped zinc oxide for resistive switching applications

Pavan Kumar Reddy Boppidi,[1] P. Michael Preetam Raj,[1] Swapna Challagulla,[2] Sankara R. Gollu,[3] Sounak Roy,[2] Souri Banerjee,[4] and Souvik Kundu[1,a)]

[1]*Department of Electrical and Electronics Engineering, Birla Institute of Technology and Science (BITS) Pilani, Hyderabad Campus, Hyderabad 500078, India*
[2]*Department of Chemistry, Birla Institute of Technology and Science (BITS) Pilani, Hyderabad Campus, Hyderabad 500078, India*
[3]*School of Electrical and Electronic Engineering, Nanyang Technological University, Singapore 639798, Singapore*
[4]*Department of Physics, Birla Institute of Technology and Science (BITS) Pilani, Hyderabad Campus, Hyderabad 500078, India*

(Received 20 August 2018; accepted 8 November 2018; published online 3 December 2018)

In this study, efforts were devoted to unveiling the dual role of single crystalline Cu (5%) doped ZnO (Cu:ZnO) synthesized by a simple and low-cost chemical process and to investigate its efficacy on resistive switching (RS) applications. It was found that when Cu:ZnO was annealed at a lower temperature of 450 °C and integrated onto ITO/glass for RS applications, only oxygen mediated vacancies were responsible for its resistive switching. However, ferroelectric properties have been observed when the same Cu:ZnO was annealed at a higher temperature of 800 °C and integrated onto Nb doped $SrTiO_3$. X-ray diffraction, high resolution transmission electron microscope, x-ray photoelectron spectroscopy, UV-VIS-near infrared spectrometer, and piezoelectric force microscopy (PFM) were employed to study the crystallinity, interfaces, chemical compositions, bandgap, and domains in Cu:ZnO thin films, respectively. The bandgap of Cu:ZnO was found to be 3.20 eV. PFM study exhibits the domain inversion with 180° polarization inversion by applying an external bias, evidencing its effectiveness for memory applications. When the electrical characteristics were concerned, the RS device based on this ferroelectric Cu:ZnO offers better performance, such as lower SET/RESET voltages (~1.40 V), higher retention (up to 10^6 s) without distortion, and higher ON/OFF ratio (2.20×10^3), as compared to the former lower temperature annealed Cu:ZnO devices. A band-diagram was proposed, and transport studies were developed to understand the operational mechanism of these devices. This study explains both the limits and scopes of Cu:ZnO RS devices and formulates an idea which may accelerate the design of future generation devices. *Published by AIP Publishing.* https://doi.org/10.1063/1.5052619

I. INTRODUCTION

The ever increasing demand for scalable, low power, high speed, and reliable storage devices has led to the need for alternatives, which surmount the limited advantages of widely used silicon based dynamic random access memory (DRAM), static random access memory (SRAM), and flash memory technologies.[1] Resistive switching (RS) devices, or memristors, were found to be a promising alternative to the existing flash memory technologies owing to their several advantages over other memory technologies, viz., low cost fabrication, scalability, high switching speed (5 ns), low switching voltage (<3 V), better endurance (>10^6 cycles), long retention time (10 years), and multibit operation.[2] It is the simplest top electrode-interlayer-bottom electrode structure, in which the data are stored in the form of a change in its electronic resistance.[1] The working principle of RS devices depends on the change in currents between the high resistance state (HRS) and low resistance state (LRS) in accordance with the external bias. It was found from the literature that perovskite oxides,[3] ferromagnetic materials,[4] ferroelectric materials,[5] polymers,[6] organic semiconductors,[7] and transition-metal oxides[1] (TMOs) were used as an interlayer or active material in these devices. Among these materials, TMO and ferroelectric materials are mostly preferred due to their high scalability, low cost, easy fabrication process, low power, fast switching speed, low operating voltage, and their high density integration with the existing CMOS process technologies.[2,5]

Various mechanisms such as interface barrier, formation of metallic filament (or simply formation), and trap states have been adopted in order to explain the electrical characteristics and switching operation in TMO based devices.[1,8,9] The disadvantage of the filamentary type mechanism is that it requires high forming voltage which is not suitable for low power applications.[10] In addition, frequent formation and rifting of filaments can lead to Joule heat dissipation, which ultimately degrade the performances and storage capacity of the RS devices.[10] Therefore, to overcome the abovementioned problems, it is desirable to fabricate forming free

[a)]Author to whom correspondence should be addressed: souvikelt@gmail.com and souvik.kundu@hyderabad.bits-pilani.ac.in

devices where intrinsic defects such as oxygen vacancies or ferroelectric polarizations would play a major role in the RS operation.[11] Several studies have revealed that TMOs such as ZnO, HfO_2, and TiO_2 offer excellent electrical and structural properties, and their fabrication process is compatible with the existing CMOS technology.[2,8,12] Recently, there has been renewed interest in utilising ZnO as an active layer owing to its low temperature facile synthesis process and pre-existing oxygen vacancies and ions.[13,14] Efforts have been devoted to further improve the device performances through the insertion of metal dopants into the ZnO lattices, which can modify the oxygen vacancies, ions, defect structures, and electrical conductivity.[15] Different metals were invoked in order to address this doping, such as lithium,[16] aluminum (Al),[17] copper (Cu),[15] cobalt,[18] vanadium,[19] titanium,[20] lanthanum,[21] etc. Among these dopants, Cu has the similar electron shell structure as that of zinc (Zn) making it comfortably fit into the ZnO lattice structure.[4] On the other side, Cu atoms also act as electron traps in ZnO and conquer the recombination process.[22] Furthermore, the electrons move within the Cu and oxygen bonds because of their strong covalence, which may lead to electron deficiency in the nearby Zn and oxygen bonds.[23] Few researchers attempted to develop Cu doped ZnO (Cu:ZnO) based RS devices, and they measured some essential electrical properties such as ON/OFF current ratio and switching voltages.[12,24] However, the obtained electrical parameters were still inadequate to meet the commercial demands and do not satisfactorily set the design criteria for practical RS devices. Moreover, the structural properties of the thin film, working principle of the devices, and its transport properties were not comprehensible. When the memory is concerned, one should explore the retention property of the fabricated devices to observe the charge decay principle. Unfortunately, the retention of the devices was limited to only 10^4 s (studied by Kim *et al.*), which is not efficient to contend with the flash memory devices.[24] In addition, it is also essential to understand (i) the efficacy of Cu ions, (ii) the role of oxygen vacancies in the RS mechanism, and (iii) their correlation with the switching measurements to explain the macroscale electrical properties. Therefore, not much work has been performed in elucidating these and this gap retains the scope for further investigation.

It was found that Cu could be the electron trap in ZnO, may increase its resistivity, and act as a ferroelectric material.[22,25] Therefore, Cu:ZnO attributes its dual property; it can be used as a TMO as well as a ferroelectric material. Recently, there have been tremendous research efforts for developing ferroelectric material based RS or other electronic devices owing to its polarization and polarization inversion properties.[5,26–28] It is important to mention that in ferroelectric based devices, the absence of electroforming or filament formation may lead to improved lifetime with better switching properties.[5] On the one side, the data writing and reading in ferroelectric based RS devices are made possible through inversing the ferroelectric polarization domains, which is a much faster process as compared to any other memories.[5,27] On the other side, one can perform the RS operation in a ferroelectric material by utilizing an external electric field beyond its coercive field.[29] Thus, in order to fabricate a low-power and fast RS device, one should use a suitable ferroelectric material, which possesses low coercive field, high polarization, and domain inversion.[5] Several researchers put their efforts to establish the ferroelectricity in Cu:ZnO.[9,25,29,30] In this regard, Su and Zhang studied the trapped charges in Cu:ZnO using scanning probe microscopy.[9] On the other hand, Xiao *et al.* utilized piezoelectric force microscopy (PFM) to investigate the polarization rotation in Cu:ZnO.[29] The multiferroic properties in Cu:ZnO were also studied for possible electronic applications.[4,25,30] However, these authors neither fabricated any meaningful memory devices to demonstrate the electrical performance nor made a correlation with their microscopy data to the device level quantifications. In order to get the benefits of ferroelectric properties, Xiao *et al.* extended their study to reveal the electrical characteristics of ferroelectric Cu:ZnO using the conductive atomic force microscopy (C-AFM) technique.[12] In their study, platinum was used as the bottom electrode, whereas the C-AFM tip was utilized for the purpose of the top electrode (*in situ*). Interestingly, the authors have not fabricated any *practical* RS devices; instead, they only depended upon their *in situ* C-AFM measurements. Their results offer a low ON/OFF ratio and high SET/RESET voltages, both are detrimental for RS applications as the high ON/OFF ratio is essential for a fast reliable operation, whereas lower SET/RESET voltages are desirable for low power applications.[5] In addition, the desired correlation between their microscopic [PFM, SPM (scanning probe microscope), and C-AFM] results and the electrical properties is also limited. Although the study of multiferroic properties in Cu:ZnO is much celebrated, however, there is no attempt yet to develop any practical RS devices by imposing the ferroelectric properties in Cu:ZnO. Moreover, one should carefully study the band-diagram in order to understand the device operation principle (SET/RESET process). Therefore, insufficient information on domain kinetics coalesced with the limited understanding of the devices' write-read-program-erase operations opens up a scope for a systematic study that can overcome the abovementioned aspects. Furthermore, in order to gain insight into the charge transport properties in the metal/ferroelectric interface, it is crucial to lay down a framework to reveal the domain switching principle and make a correlation with the electrical performances, which would provide a comprehensive understanding for the commercial translation.

This study explains a new approach where the dual role of Cu:ZnO was revealed based on low-cost and solution-process techniques. First, we investigate the forming free Cu:ZnO based RS devices integrated onto the ITO/glass substrates, where Al was used as the top electrode. The chemical route was adopted to synthesize the single crystalline Cu:ZnO as it induces several advantages such as low processing temperature, inexpensive, and simple procedures, suitable for large area applications, and most importantly, it does not require high vacuum like other sophisticated equipment. The annealing temperature of Cu:ZnO was maintained low (450 °C) and this also prevents cross contamination from the glass substrates. The electronic band-diagrams of these RS devices during SET and RESET operations were

proposed, and a systematic investigation was conducted to reveal the electrical performance of these devices. The role of Cu in the oxide material was elaborated through vacancy mediated concepts. Later, the same composition of Cu:ZnO was annealed at higher temperature (800 °C) and heterogeneously integrated onto niobium doped strontium titanate (Nb:STO) substrates to observe its ferroelectricity. Nb:STO can be used to grow oxide thin films since it can sustain higher temperatures (where glass cannot) and avoid cross talk due to its semiconducting properties.[5] The absence of cross talk may further enhance the device scalability, and no additional rectifying devices were required, which ultimately reduces the overall power consumption.[5,31] PFM was utilized to interpret the domain switching in Cu:ZnO, and high-resolution transmission electron microscopy (HRTEM) was used to analyze the interface with Nb:STO. PFM results expose the repeatable 180° polarization inversion by poling, affirming its potential for read-write operation in memories. Ferroelectric Cu:ZnO based RS devices were fabricated, which exhibit higher retention time, lower coercive voltage, higher ON/OFF current ratio, and reliable operation as compared to the former Al/Cu:ZnO/ITO/glass devices. Efforts were devoted to elucidating the underlying cause for these meliorations. Furthermore, a correlation was established between the structural and electrical results, and a band-diagram was projected to explicate the operational principles in these ferroelectric based RS devices.

II. MATERIALS AND METHODS

A. Material preparation

The Cu:ZnO was synthesized using inexpensive chemical techniques. In order to achieve the solution of Cu:ZnO, 0.30 M zinc acetate solution was prepared by adding 0.6585 g of zinc acetate di-hydrate (purchased from SRL, India) to 10 ml of isopropanol. Di-ethanolamine (DEA, purchased from AVRA, India) was utilized as a stabilizing agent, and the molar ratio of Zn^{+2}:DEA was maintained to 1:1 (0.298 ml). This solution was stirred for 600 s. 5% of copper (II) acetate solution was developed by adding 29.94 mg of copper (II) acetate monohydrate (purchased from SRL, India) to the prepared zinc acetate solution and then stirred for 2 h at 60 °C. The entire solution was aged for 22 h.

B. Device fabrications and characterizations

In order to fabricate Al/Cu:ZnO/ITO/glass and Pt/Cu:ZnO/Nb:STO RS devices, first $1 \times 1\ cm^2$ ITO/glass and Nb:STO substrates were degreased with acetone, followed by rinsing in isopropyl alcohol and then ultra-sonicated in DI water for 3 min. The solution of synthesized Cu:ZnO was spin coated onto both ITO/glass and Nb:STO substrates at 3000 rpm for 30 s to achieve 50 nm thickness. After spin-coating, to get the better adhesion, the thin film of Cu:ZnO onto ITO substrates was immediately dried at 120 °C for 600 s inside a rapid thermal processor under nitrogen ambience. The samples were then annealed at 450 °C for 1 h in air, whereas, in order to achieve the ferroelectric property in Cu:ZnO, the deposited thin film onto Nb:STO substrates was annealed at 800 °C under O_2 partial pressure (350 mTorr). Ellipsometer and cross-sectional HRTEM were utilized to confirm the thickness (50 nm) of the deposited Cu:ZnO. The surface morphology of the film was studied by AFM and field emission scanning electron microscope (FESEM). HRTEM and x-ray photoelectron spectroscopy (XPS) were utilized to study the interface of Cu:ZnO with the substrates. Al top electrodes were developed onto Cu:ZnO/ITO/glass using a thermal evaporator, and a shadow mask was utilized to obtain the pattern. However, the sputtering technique was employed to deposit Pt onto Cu:ZnO and In at the backside of Nb:STO. In provides low contact resistance from the Nb:STO substrates. Ferroelectric Polarization–Electric field (P-E) measurement was performed using the modified Sawyer-Tower Bridge technique. PFM was used to establish the ferroelectricity and polarization inversion in the film deposited onto the Nb:STO substrates. The out-of-plane piezoresponse and local hysteresis loops were recorded by PFM using a scanning probe station. The AC drive amplitude was maintained at 1000 mV (290 kHz) throughout the DC bias sweep. The room temperature electrical properties of both the devices were recorded using a Keysight B2912A source meter.

III. RESULTS AND DISCUSSION

X-ray diffraction (XRD) was utilized to identify the crystalline nature of the Cu:ZnO thin films. Figure 1(a) shows a sharp peak along the (002) orientation at an angle (2θ) of 35°, which resembles the single crystalline thin film deposited onto the ITO/glass substrate. Interestingly, in the XRD plot, there are no additional impurity peaks or secondary Cu associated phases present, and the obtained results were well matched with the other reported literature.[32,33] The absence of other secondary phases may depict that the atomic radius of Cu is in close match with that of Zn; thus, its

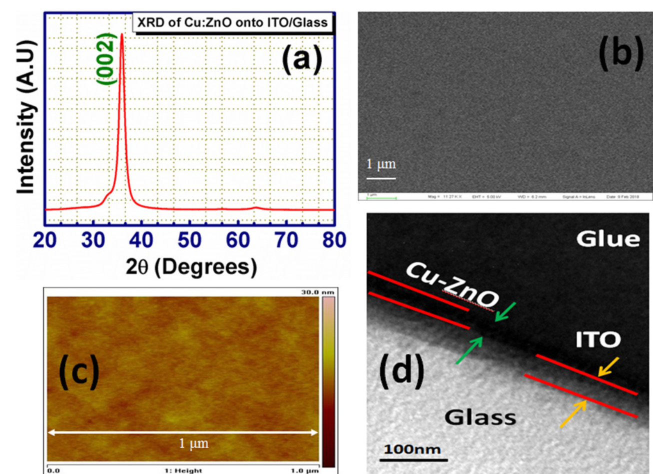

FIG. 1. (a) XRD pattern of Cu (5%):ZnO thin film (annealed at 450 °C) deposited onto the ITO/glass substrate. The pattern indicates the single crystalline structure of Cu:ZnO without any secondary defect states. The surface morphology of sol-gel spin coated Cu:ZnO (b) FESEM image and (c) AFM image. Both the micrographs depict the smoothness of the deposited film without voids. (d) Cross sectional high resolution transmission electron micrograph of Cu:ZnO, ITO, and glass. The image shows that a homogeneous thin film was formed onto the substrate.

incorporation into the ZnO lattice is feasible, without altering its wurtzite structure. However, the thin film exhibits the preferred orientation in the (002) direction, which is consistent with the growth along the *c* axis. Field emission scanning electron microscope (FESEM) and atomic force microscope (AFM) were used to study the surface morphology of the Cu:ZnO thin film deposited onto the ITO/glass substrate and it is depicted in Figs. 1(b) and 1(c), respectively. From these micrographs, one can see that no voids or pit holes are present on the films which indicate uniform distribution, which is in agreement with the XRD result. The surface roughness of the deposited film was found to be negligible (0.22 nm), thus avoids any chances of leakage. Since the interface between the active material and substrate plays a pivotal role in the device performance, HRTEM was utilized to show the cross-sectional interface of Cu:ZnO onto the ITO/glass substrate. The obtained micrograph [shown in Fig. 1(d)] indicates defect free interfacial layer and chemical stability in the deposited film. Also, no inter-diffusion of impurity layers is found from the glass substrate. The interface between them was found to be homogeneous, which may further enhance the device performance. The thickness of Cu:ZnO was measured to be 50 nm, which exactly matches with the result obtained from the ellipsometer. It is noteworthy to mention that the abovementioned attributes were accomplished by carefully controlling the Cu composition, growing a high quality thin film, and lowering the defect density.

X-ray photoelectron spectroscopy (XPS) was employed to identify the chemical compositions in Cu:ZnO. All the binding energies were adjusted for the sample charging effect with reference to the C_{1s} line at 284.50 eV. Figure 2(a) shows the Cu_{2p} XPS spectrum of the Cu:ZnO thin film. The Cu_{2p} signal comprises two peaks located at 932.6 eV and 952.4 eV, which indicate $Cu_{2p3/2}$ and $Cu_{2p1/2}$ spin orbital splitting (SOS), respectively. The SOS of the Cu_{2p} was found to be 19.8 eV. The presence of ZnO was observed by the Zn_{2p} and O_{1s} spectra and is shown in Figs. 2(b) and 2(c), respectively. The peaks at 1021.9 eV and 1045.1 eV were attributed to $Zn_{2p3/2}$ and $Zn_{2p1/2}$, respectively, with the SOS of 23.2 eV. The peak located at 531 eV corresponds to the O_{1s} spectrum, i.e., the O^{2-} ions, which were surrounded by Zn atoms in the wurtzite structure.[34] The relations for native defect generation in nonstoichiometric ZnO can be written as[18]

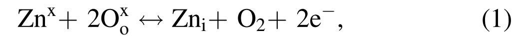

$$Zn^x + 2O_o^x \leftrightarrow Zn_i + O_2 + 2e^-, \quad (1)$$

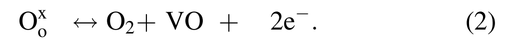

$$O_o^x \leftrightarrow O_2 + VO + 2e^-. \quad (2)$$

The above relations represent the formation of oxygen vacancies and ions in the ZnO lattices. Zn^x, O_o^x, and VO are considered as the internal defects in ZnO, where Zn^x and O_o^x indicate the neutral charge of Zn and O ions, respectively. Zn_i is believed to be the positive charge of Zn in its interstitial site. It was understood that ZnO shows as grown n-type behavior due to the presence of Zn_i and VO defects in it.[18,35] However, proper incorporation of the Cu dopants into the ZnO lattice indicates the formation of an (Cu_{Zn}–VO) acceptor complex, which may result in p-type conductivity in Cu:ZnO. The presence of p-type conductivity in Cu:ZnO was further confirmed using Hall and hot-probe measurements. The generation of native defects in ZnO can be analyzed through the broken chemical bonds in its crystal structure. According to Biswas *et al.*[36] and Tay *et al.*,[37] the binding energy (BE) peak of $Zn_{2p3/2}$ at 1022 eV can be attributed to the stoichiometric ZnO, i.e., Zn ions are tetrahedrally surrounded by four oxygen ions at different lattice points. It was also understood that the increase in the number of broken bonds may lead to an increase in the oxygen vacancies.[37] In the present study, the BE shifted left side from 1022 eV [as shown in Fig. 2(b)] and imputed to weakening of charge transfer between Zn and O ions, which resulted in three oxygen ions with a broken bond.[36] In addition, the O1s peak at 531 eV confirms the presence of oxygen vacancies in the Cu:ZnO thin film.[36,38] Thus, lowering in the BE value may be due to the incorporation of Cu into the ZnO lattice, which further results in an increase in the number of oxygen vacancies and defect states. In this process, more electrons will be trapped into ZnO, which helps one to retain the charges inside these trapped states.

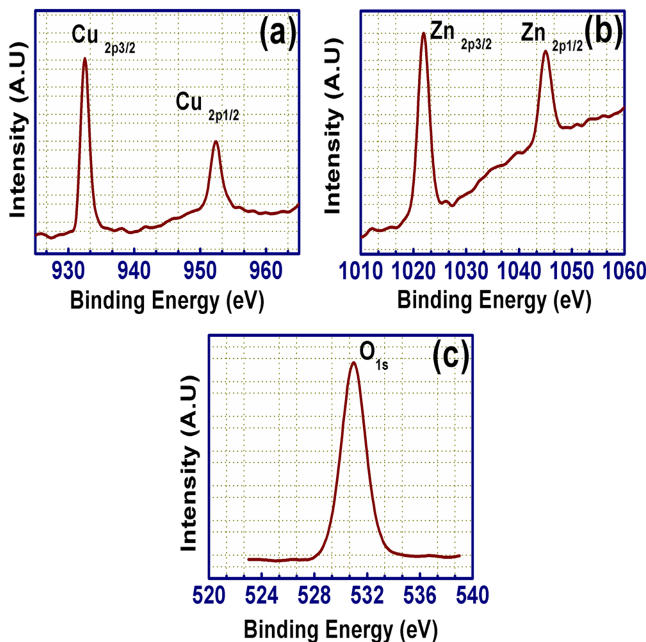

FIG. 2. XPS of (a) $Cu_{2p3/2}$ and $Cu_{2p1/2}$, (b) $Zn_{2p1/2}$ and $Zn_{2p3/2}$, and (c) O_{1s}. The spectra identified all the available peaks that correspond to Cu, Zn, and O elements.

The deposited Cu:ZnO thin film onto ITO/glass substrates was found to be transparent and is shown in Fig. 3(a). In order to understand the RS device operation principle, it is very important to establish the band-diagram of Cu:ZnO sandwiched between two electrodes, where the bandgap of the active material would play a key role. In this regard, the UV-VIS-NIR (near infrared) spectrometer was used to obtain the absorption spectrum of Cu:ZnO and a sharp absorption peak around 359 nm was located, which is attributed to the direct band-to-band transition. A clear red shift is observed and this shift is due to the doping of Cu into ZnO.[39] Well known Tauc's plot [$(\alpha h\nu)^2$ vs. $(h\nu)$] has been utilized to

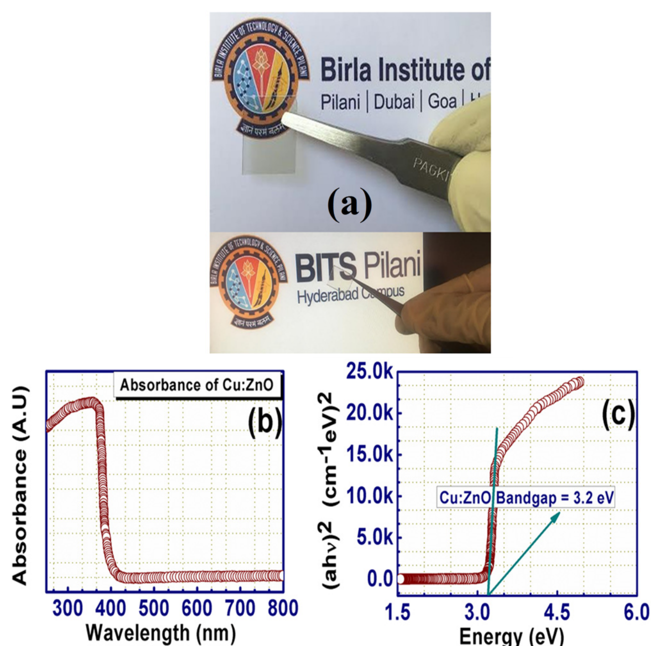

FIG. 3. (a) Cu:ZnO thin film deposited on the ITO/glass substrates, and the film was found to be transparent. (b) Absorption spectra of Cu:ZnO obtained through the UV-VIS-NIR spectrometer. The absorption peak at 359 nm is observed to be in the visible region. (c) The $(\alpha h\nu)^2$ vs $(h\nu)$ Tauc plot, which was constructed from the absorption spectra. The direct bandgap of Cu:ZnO was found to be 3.20 eV.

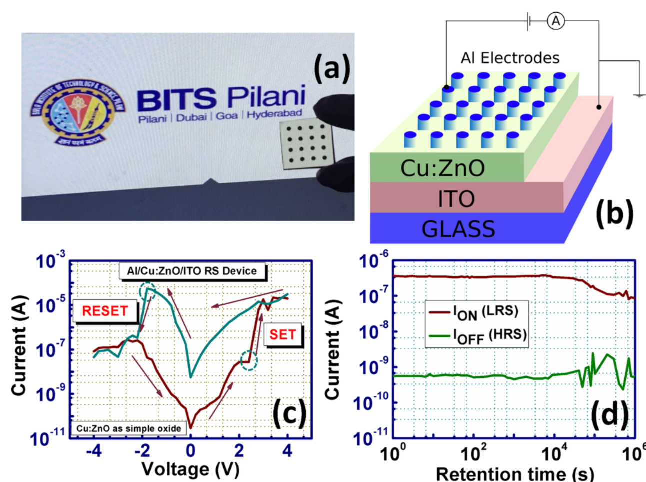

FIG. 4. (a) Fabricated Al/Cu:ZnO/ITO/glass RS devices. It can be seen that the devices are transparent with opaque Al electrodes. (b) Schematic of the fabricated device architecture. (c) Current vs voltage (*I-V*) characteristics of the RS device. The voltage was swept from 0 to 4 V, 4 to 0 V, 0 to −4 V, and back −4 to 0 V. The SET and RESET occur at 2.40 V and −1.80 V, respectively. (d) Data retention of the fabricated RS device. The retention was stable up to 10^4 s and started degrading beyond this time.

determine the direct bandgap of Cu:ZnO, and the value was found to be 3.20 eV, which is lower than that of the conventional ZnO (3.37 eV).[32,34] Thus, the lowered bandgap in Cu:ZnO resembles that the concentration of Cu impurities creates localized states, which are defects caused by the unsaturated bonds. In our previous study, photo luminescence (PL) spectra showed a defect emission, which was attributed to the reduced electron-hole recombination at trapped defect sites in the ZnO thin film, which may lead to lowering of the energy bandgap.[40]

In order to observe the RS effects in 450 °C processed Cu:ZnO, aluminum (Al) was employed onto it as a top electrode, whereas ITO served the purpose of a bottom electrode. The actual fabricated device image is shown in Fig. 4(a), where Fig. 4(b) refers to the device's schematic. The room temperature current-voltage (*I-V*) properties were recorded in Al/Cu:ZnO/ITO/glass RS devices [Fig. 4(c)]. From the figure, one can see that the voltage was varied from 0 to 4 V and then brought back from 4 to 0 V and then again swept from 0 to −4 V and finally returned to 0 V. The switching mechanism was understood from the change in its current from HRS to LRS and LRS to HRS. Initially, when there is no applied bias, the device is in HRS. When a positive bias was applied from 0 V, the device remained in HRS until 2.40 V, at which the current was found to be 2.73×10^{-8} A. Interestingly, when the bias was continued to vary from 2.40 V to 4 V, the current gradually increased to 1.95×10^{-5} A, referring the LRS. Therefore, this 2.40 V was identified as the SET voltage. Prior to this measurement, a current compliance of 1 mA was set in order to avoid the accidental dielectric breakdown of the devices. Furthermore, the voltage was driven back from 4 to 0 V, the device remained in LRS, and the current at SET voltage was found to be 7.87×10^{-6} A. When the polarity of the bias was changed and swept from 0 to −4 V, the device started to switch back from LRS to HRS at −1.80 V. Initially, the current at −1.80 V was measured to be 5.58×10^{-5} A. However, when the bias was further increased from −1.80 V to −4 V, the device gets settled in HRS and it continued to persist in this state even with the change in the applied bias from −4 to 0 V, confirming the bipolar nature of the devices. Therefore, the SET/RESET voltage was found to be 2.40/−1.80 V, respectively. It is noteworthy that the switching processes in our devices are free from the formation of conductive bridge filaments or any other electroforming process. Since large current and voltage are required for inducing such a forming process in other oxides or solid electrolyte based devices, our present approach saves the devices from thermal damage and thereby enhances its reliability.[5] It is crucial to determine the ON/OFF ratio to analyze the device performance in terms of its reliability and throughput. The ON/OFF ratio is defined as the ratio of the ON current in LRS and the OFF current in HRS, and it was found to be 656 at 1 V. Since the primary application of these RS devices is non-volatile memory (NVM), it is indispensable to characterize out the retention property of the fabricated devices, which is nothing but to study the variation of HRS and LRS currents as a function of time. This property was measured by biasing the devices at 1 V (withdrawn after 60 s) and the result is shown in Fig. 4(d). Surprisingly, the device demonstrates stable charge retention for 7×10^3 s and then started degrading. However, it still conserves the separation of LRS and HRS and maintains a moderate ON/OFF ratio (656). In order to gain insight into the transport properties in our fabricated Al/Cu:ZnO/ITO/glass RS devices, conduction mechanisms were ascertained through fitting both the HRS and LRS *I-V* curves and are shown in Fig. 5. It was found that several carrier injection mechanisms are responsible for the current transport in RS

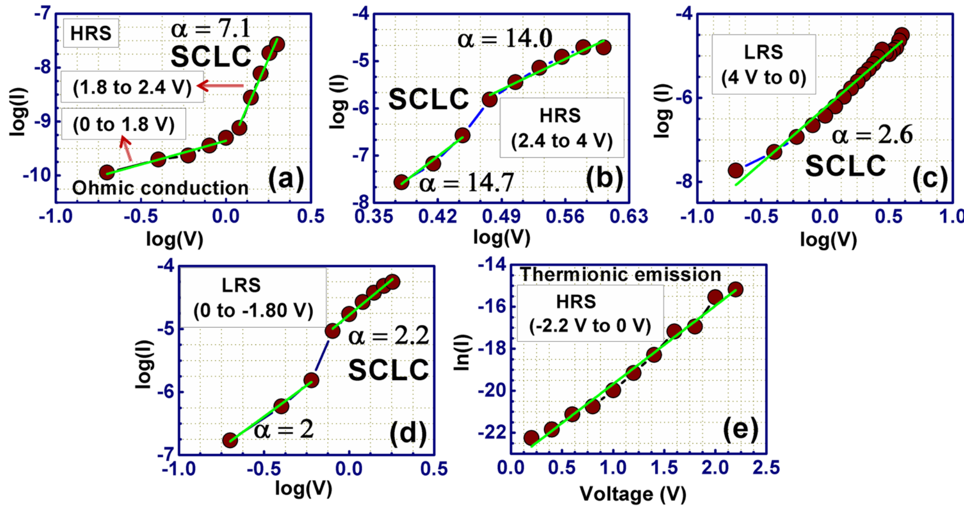

FIG. 5. Identification of the conduction mechanism in the Al/Cu:ZnO/ITO/glass based RS device: (a) 0 to +2.40 V HRS, (b) 2.40 V to 4 V HRS, (c) 4 V to 0 V LRS, (d) 0 to −1.8 V LRS, and (e) −2.20 V to 0 V HRS. The slope (α) was found to be greater than 2 in most of the cases, which refers that the conduction is governed by the SCLC mechanism, whereas Ohmic conduction and thermionic emission were responsible for 0 to 1.80 V HRS and −2.20 V to 0 V HRS, respectively.

devices: (i) Ohmic conduction where $I \propto V$, (ii) thermionic emission where $\ln I \propto V$, (iii) space charge limited current (SCLC) where $I \propto V^{\alpha}$ and $\alpha \geq 2$, (iv) Poole-Frenkel emission where $\ln(I/V) \propto V^{1/2}$, and (v) Fowler-Nordheim tunneling, where $I \propto V^2\exp(-E_a/V)$ (E_a is the kinetic energy of the charge carriers).[5] During HRS and LRS at a positive applied bias, the SCLC was responsible for current transport when the voltage was varied from 0 to 4 V [Figs. 5(a)–5(c)]. SCLC also acted to be the cause for the transport mechanism during LRS when the voltage was swept from 0 to −1.80 V [Fig. 5(d)]. However, one can observe that the voltage range from −1.80 to −4 V is referred as a negative resistance region for both LRS and HRS. For this region, the most probable cause for the transport could be the non-frontier states, which provide channels and the charge can be transported across the interface of metal/TMO.[41,42] Moreover, the trapped electrons can be swept out from their trapping centres and are stimulated toward the anodic side, colliding with various scattering centres within the ZnO. Finally, the thermionic emission comes into play when the voltage was reduced from −2.20 to 0 V, which is shown in Fig. 5(e).

It is inevitable to investigate the RS mechanism in Al/Cu:ZnO/ITO/glass devices; therefore, a transport model was proposed (shown in Fig. 6), which describes the most probable cause for RS behavior. When a positive bias was applied on the top Al electrode, O^{2-} ions get moved to the metal/TMO interface leading to the formation of the AlO_x layer, which allows the device to be in the HRS initially and then jump to LRS due to the aggregation of O^{2-} ions. On the other hand, when a negative bias was applied on the top electrode, positively charged oxygen vacancies, i.e., VO^{2+} displaced toward the top electrode through dissolving the AlO_x layer. This ensues drastic change in current and leads to LRS initially and jumps back to HRS due to repulsion of O^{2-} ions. Similar effects have also been observed in ZnO based RS devices.[43,44] This affirms that the SET and RESET processes were based on the migration of oxygen ions and vacancies in the metal/TMO interfaces, thus offers better stability and reliability as mentioned earlier. The memory mechanism was also due to carefully doping of Cu into the ZnO lattice, which leads to the formation of a large number of vacancies and defect states as was discussed in the XPS section.

Since invoking of Cu into the ZnO lattice may introduce ferroelectricity, efforts were consecrated to study its role in the RS mechanism. However, establishment of ferroelectricity in a material and realization of practical devices are not straightforward. In this regard, one should use a suitable single crystal material, which possesses low coercive field, high polarization, and expresses its domain inversion. Figure 7(a) shows the XRD pattern of the higher temperature annealed (800 °C) Cu:ZnO onto the Nb:STO substrate. The two dominant peaks with orientations (001) and (200) at angles (2θ) 22° and 46° indicate the single crystalline Nb:STO, whereas the Cu:ZnO thin film was also found to be

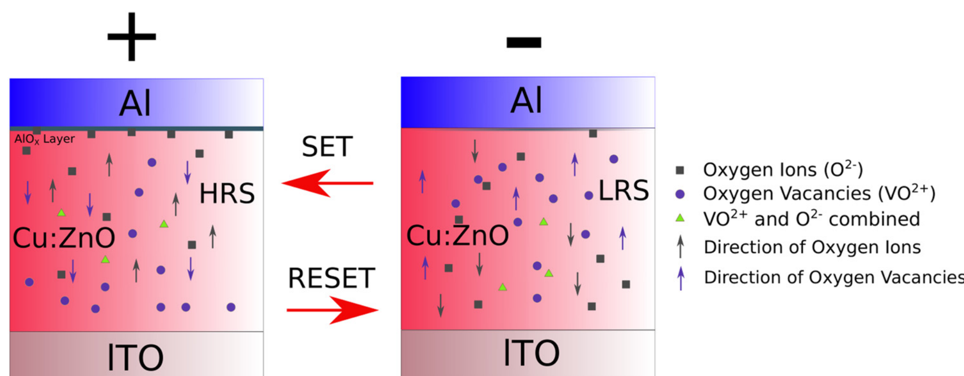

FIG. 6. Schematic of the transport mechanism of the forming free Al/Cu:ZnO/ITO/glass device. Under the applied bias, O^{2-} and VO^{2+} ions move in a direction within the device, which depends on the polarity of the applied voltage. This model explains the reason for switching between HRS and LRS.

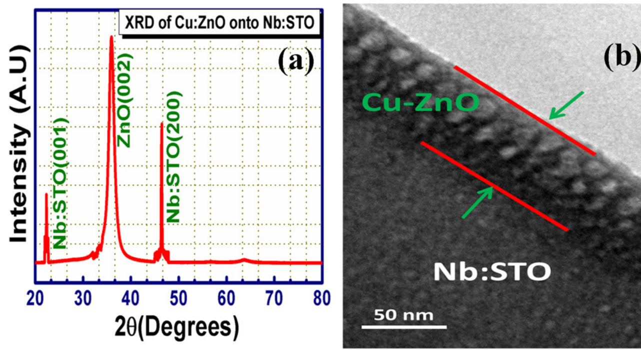

FIG. 7. (a) XRD pattern of Cu (5%):ZnO thin film deposited onto the Nb:STO substrate and annealed at 800 °C with O_2 partial pressure. The peaks showcase the single crystalline formation of Cu:ZnO thin film onto the Nb:STO substrates. (b) Cross sectional HRTEM image of the Cu:ZnO/Nb:STO interface. A uniform layer of Cu:ZnO can be seen on top of the Nb:STO substrate.

single crystalline as evidenced from its (002) orientation at an angle (2θ) of 35°. In the XRD pattern, no additional diffraction peaks were observed, which confirm the purity of the deposited film.[45–48] The peak broadening of ZnO can be attributed to the inclusion of Cu dopant. The Cu:ZnO/Nb:STO interface was analyzed using HRTEM and is shown in Fig. 7(b). The smooth and homogeneous interface between the two stacks confirms the deposition of a high quality film onto the Nb:STO substrate. The thickness of the Cu:ZnO was ascertained to be 50 nm (from the ellipsometer and HRTEM).

PFM was utilized to study the ferroelectricity and their switching behavior in higher temperature processed Cu:ZnO. It was interpreted that in order to establish the ferroelectric property, 180° domain inversion is inevitable, which further sets the way to make the material ready for potential RS applications.[27,49] Thus, the investigation of domain formation and the demonstration of polarization inversion offer a promising approach toward the design of a futuristic ferroelectric based RS devices. In the PFM study, the lateral PFM was carried out to obtain the micrographs of topography, phase angle, and amplitude. Figure 8(a) shows the PFM topography recorded from the surface of the film. The small patches with two different colour contrasts (yellow and maroon) were observed, and these can be considered as ferroelectric domains with opposite polarizations (by 180°). In order to perform the write operation, $\sim 1 \times 1\,\mu m^2$ region was positively [as shown in Fig. 8(b)] and negatively [Fig. 8(c)] poled through an external bias and read with the $2 \times 2\,\mu m^2$ region. Both the figures illustrate the colour disparity in the central $1 \times 1\,\mu m^2$ region as compared to the remaining portion of the $2 \times 2\,\mu m^2$ area. One may observe that the maroon regions were changed to yellow during positive poling inside the $1 \times 1\,\mu m^2$ region. On the other side, during negative poling of 5 V, the same inner region was turned back into the maroon region. Therefore, the change of colours in the specified regions provides the direct evidence for polarization inversion in Cu:ZnO. To repeat this process more efficiently, the polarization inversion was further observed by poling the inner $0.5 \times 0.5\,\mu m^2$ region, with −5 V and the outer $1 \times 1\,\mu m^2$ by 5 V [Fig. 8(d)]. Therefore, the

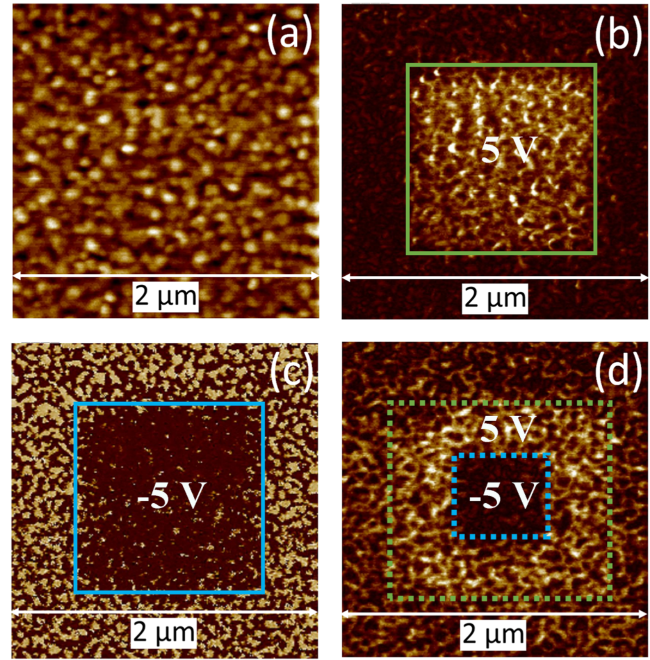

FIG. 8. Ferroelectric polarization switching in the Cu:ZnO ferroelectric material. PFM micrographs for (a) surface topography, domain inversion after poling with (b) +5 V, (c) −5 V, and (d) ±5 V applied bias. The polarization inversion can be identified by the change in the colour of the microscopy image, which indicates its effectiveness for domain switching.

ferroelectric domains are not pinned, and the two distinct colours in these regions indicate the repetitive switching of domains. Demonstration of this polarization inversion in Cu:ZnO was very critical in order to realize its efficacy for RS device applications. The ferroelectric behavior of the film is also evident from the hysteresis loops obtained from the P-E, amplitude, and phase plot as shown in Figs. 9(a)–9(c), respectively. The P-E plot was recorded at room temperature with 0.50 kHz frequency, and it depicts a clear hysteresis loop. The result also indicates that Cu:ZnO exhibits adequate

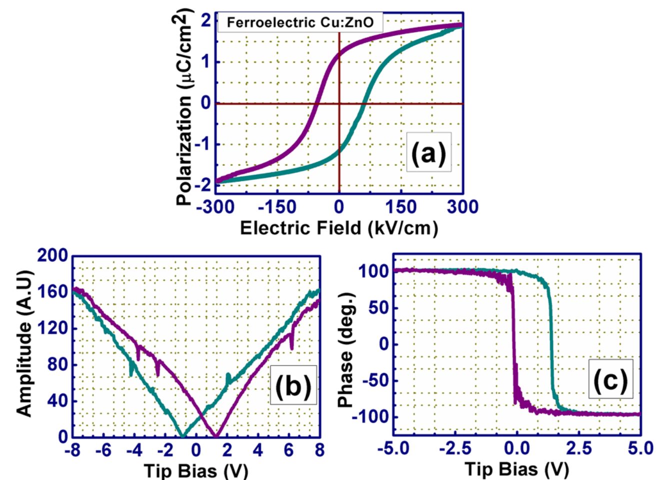

FIG. 9. Hysteresis behavior of Cu:ZnO obtained from P-E measurement and PFM. (a) Polarization–electric field, (b) amplitude, and (c) phase loop results depict the hysteresis behavior in the material. Amplitude results exhibit the low coercive voltages, whereas 180° polarization inversion was observed from the phase analysis.

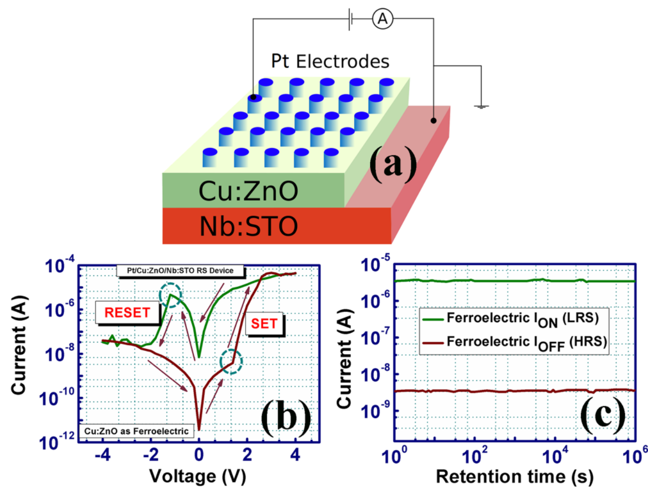

FIG. 10. (a) Schematic of the proposed Pt/ferroelectric Cu:ZnO/Nb:STO device. (b) The *I-V* characteristics are measured by sweeping the voltage range from 0 to +4 V, +4 to 0 V, 0 to −4 V, and −4 to 0 V. The SET/RESET voltages were found to be ±1.40 V, which overlaps with the obtained coercive voltage. (c) Charge retention property of the devices. The device offers better retention property for a longer duration (>10^6 s).

high resistivity for the ferroelectric polarization switching, which was further confirmed by PFM studies.[4] Both the PFM amplitude and phase results [Figs. 9(b) and 9(c)] exhibit a sharp 180° inversion, which clarifies that the polarizations can be switched to upward or downward direction by an external bias.[50] From the butterfly shaped amplitude results, the coercive voltage was found to be ±1.10 V. This low value of coercive voltage refers that the ferroelectric Cu:ZnO may be suitable for low power applications. The origin of ferroelectricity in Cu:ZnO is due to both Cu dopant and oxygen vacancies. The Cu dopant exists in two oxidation states of Cu^{2+} (ionic radius 0.72 Å) and Cu^{1+} (ionic radius 0.6 Å) inside ZnO.[51,52] On the one side, the ionic radii of Cu in both the states were smaller as compared to Zn^{2+} (0.74 Å). Thus, Cu^{1+} occupies the Zn sites and creates oxide ion vacancies.[4] On the other side, the role of oxygen vacancy is predominant in the ferroelectric behavior as it causes the Cu to lose its bonding which results in Cu–O bonds (when annealed at higher temperature) that are free to move under the external electric field. Therefore, the oxygen vacancies alter the bonding in order to create electric dipoles which lead to polarization switching and hysteresis in the Cu:ZnO, as observed in the PFM studies.[4,29] This could indicate that the surface polarization charges in Cu:ZnO are neutralized by the oxygen vacancies.[53,54]

Earlier, it was seen that the oxide (Cu:ZnO was annealed at 450 °C) based RS devices exhibit moderate ON/OFF ratio and switching voltages (as shown in Fig. 4), but the retention property degraded with time. Later, the Cu:ZnO was annealed at higher temperature (800 °C) and it was integrated onto the Nb:STO substrate. Since the material started showing ferroelectricity (as shown in Figs. 8 and 9), it would be interesting to fabricate RS devices and investigate its electrical characteristics to clearly observe the effectiveness of the ferroelectricity on device performances. To address this, Pt/Cu:ZnO/Nb:STO RS devices were fabricated and Fig. 10(a) depicts its schematic. It is important to mention that Al was replaced by Pt for the top electrode. Earlier, it was ascertained that O^{2-} ions get moved to the metal/TMO interface and introduce AlOx, which participates in the switching mechanism. However, in this case, to suppress the role of other interfacial effects and only to observe the efficacy of standalone ferroelectric material on the switching mechanism, Pt was employed instead of Al as the formation of PtOx is not possible. The *I-V* characteristic of the devices is shown in Fig. 10(b). The results exhibit similar bipolar behavior as was seen in the former Al/Cu:ZnO/ITO/glass devices. The currents demonstrate stable switching characteristics which manifest its potential for RS applications. The inception of this switching property is due to the presence of ferroelectric Cu:ZnO sandwiched between top and bottom electrodes. However, the SET (1.40 V) and RESET (−1.20 V) voltages were found to be much lower as compared to the earlier devices, which is in good agreement with the obtained coercive voltages of ±1.10 V (Fig. 9). Since the SET/RESET voltages are coupled with the same coercive voltage, a correlation can be drawn between ferroelectric and electrical properties of the same RS devices. Interestingly, the obtained low values of SET/RESET voltages set the devices to use for low-power applications. The

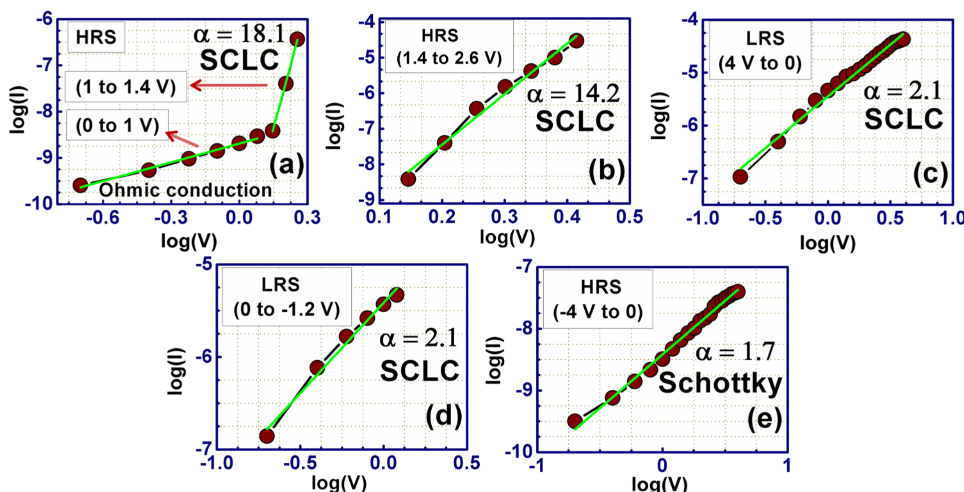

FIG. 11. Curve fitting techniques to identify the conduction mechanism in the proposed ferroelectric RS device for the cases of (a) 0 to 1.40 V in HRS, (b) 1.40 V to 2.60 V in HRS, (c) 4 V to 0 in LRS, and (d) 0 to −1.2 V in LRS. The $\alpha > 2$ indicates the SCLC based conduction mechanism, whereas $I \propto V$ indicates Ohmic conduction. (e) −4 V to 0 in HRS has an α value of 1.7, which identifies the Schottky conduction.

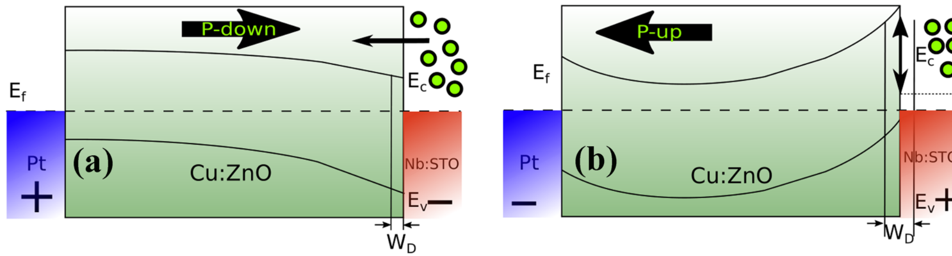

FIG. 12. Schematic of the energy band diagrams of Pt/Cu:ZnO/Nb:STO NVM devices. (a) Under forward bias condition (downward polarization) and (b) under reverse bias condition (upward polarization).

ON/OFF ratio was also significantly improved and it was found to be 2.20×10^3, which allows the devices to work faster.[5] The obtained ON/OFF ratio from our devices is considerably high when compared with other ferroelectric based devices.[26,55–57] For both LRS and HRS, the effect of polarization on the retention property was studied in current-time characteristic, which is shown in Fig. 10(c). The retention was measured up to 10^6 s and it was found to be stable throughout the measurement process. The ON/OFF ratio (in the order of 10^3) is also maintained almost constant during the measurement period. Therefore, significant improvement can be spotted in ferroelectric Cu:ZnO/Nb:STO devices as compared with the former Cu:ZnO (annealed at 450 °C)/ITO devices. All these advancements observed in the latter devices are because of both ferroelectric polarizations and oxygen vacancies, which are further elaborated subsequently in the band-diagram study. It is known that with the presence of electric field, the ferroelectric materials get spontaneously polarized and the state was maintained even when the power is turned off, showing its non-volatile property. Therefore, in the devices, ferroelectric polarization can also be the cause for high memory densities, which is responsible for better electrical performances.[49,58] In the present study, the fabricated devices are also safe from thermal damage and offer better reliability as compared to the devices where memory properties originated from the filaments or electroforming process. Again, the curve fitting techniques (Fig. 11) were utilized to identify the charge conduction mechanisms in the ferroelectric based devices. In Fig. 11(a), initially, the Ohmic conduction was responsible for the charge transport (0 to 1 V, HRS). During HRS and LRS [from Figs. 11(a)–11(d)], the charge transport was mostly governed by the SCLC mechanism. However, when the voltage range −4 to 0 V is considered [Fig. 11(e)], the Schottky conduction was identified for the HRS charge transport. Therefore, from the conduction study, it was understood that when Cu dopant is incorporated into the ZnO lattice will act as trap charges, which is indicated by the SCLC mechanism.

To understand the role of ferroelectric materials onto the device operation principle, band-diagrams were proposed with the presence of both positive and negative voltages. The doping of Nb into STO contributes additional free electrons with oxygen vacancies, which results in n-type conductivity in Nb:STO.[5] On the other hand, reduction of bandgap, increase in the Cu^{1+} concentration, and formation of (Cu_{Zn}–VO) acceptor complex lead to attain p-type conductivity in ZnO with Cu doping.[39] Therefore, a PN junction is formed with p type Cu:ZnO and n type Nb:STO with the depletion region (W_D). When a positive voltage of 4 V was employed at the top electrode [Fig. 12(a)], the ferroelectric polarization in the active layer is considered to be downward. This polarization field attracts oxygen ions from the n-type substrate and the band bends toward it, which decreases the effective barrier height. This polarization field also attracts the majority of carrier electrons from the substrate and drives back holes from the active layer. As a result, the W_D formed between the p-Cu:ZnO and n-Nb:STO junction gets decreased. The reduction of barrier height and depletion width would allow a high current to flow across the junctions, putting the device to attain LRS. When the negative bias is concerned on the top electrode, the ferroelectric polarization changes its direction and it becomes upward [as shown in Fig. 12(b)]. This polarization will now rebuff the accumulated electrons from the junction and attract holes toward the Cu:ZnO, which resulted in the increase of W_D. Since the band bends upward, no further oxygen ions can be migrated from the substrate to Cu:ZnO. Thus, the effective current across the junctions will be lower due to the enhancement of W_D, pushing out the devices to work in the HRS from LRS. Thus, ferroelectric polarization offers a unique approach to make the Cu:ZnO/Nb:STO devices work in between HRS/LRS and LRS/HRS.

IV. CONCLUSIONS

In summary, we studied the dual role of Cu:ZnO for forming free RS applications. The UV-VIS NIR spectroscopy results show that Cu addition had an impact on the electronic conduction, as the bandgap was reduced from 3.30 eV to 3.20 eV. Initially, the Cu:ZnO was annealed at 450 °C, and it was integrated onto ITO to fabricate Al/Cu:ZnO/ITO/glass devices which exhibited only oxygen vacancy assisted RS properties. The devices present an ON/OFF ratio of $\sim 6 \times 10^2$ and a stable retention until $\sim 10^4$ s; however, they lost uniformity beyond this time, which raises concern about the practicability of these devices for random access memory (RAM) applications. Therefore, efforts were devoted to anneal the Cu:ZnO at a higher temperature (800 °C) in order to establish the ferroelectric property in it. Surprisingly, PFM results indicate that polar domains in Cu:ZnO can be read and written with 180° domain inversion by the applied voltage, which confirms their potential for RAM applications. Thereafter, RS devices were fabricated to investigate the efficacy of ferroelectric property on the device performance. Excellent switching property was obtained with a low coercive voltage and a relation was accomplished with its electrical properties. The SET/RESET voltages were found to be very low ∼1.40 V, which offers their adoptability

for low power device applications. The ON/OFF ratio (about 3 times higher) and retention properties were significantly improved in ferroelectric RS devices. Furthermore, band-diagrams were proposed to explain the operation principle of the devices. It was ascertained that both the ferroelectric properties and vacancy states were responsible for the performance improvement in RS devices. Therefore, unveiling the dual role of Cu:ZnO and their performance analysis would open up new possibilities to develop a forming free, high performance, and low power non-volatile memories.

ACKNOWLEDGMENTS

The authors P.K.R.B., S.B., and S.K. acknowledge the financial support from BRNS, DAE, Government of India through Project No. 34/14/11/2017-BRNS/34286 to accomplish this work. P.M.P.R. and P.K.R.B. also acknowledge the Ph.D. fellowship support from UGC through NET JRF and BRNS, Government of India, respectively. P.K.R.B. is thankful to IIT and Ansh Rupani for providing some technical help. All authors are also thankful to BITS-Pilani Hyderabad Campus for all the support.

[1]D. Ielmini, Semicond. Sci. Technol. **31**, 063002 (2016).
[2]H. Y. Lee, P. S. Chen, T. Y. Wu, Y. S. Chen, C. C. Wang, P. J. Tzeng, C. H. Lin, F. Chen, C. H. Lien, and M.-J. Tsai, in *2008 IEEE International Electron Devices Meeting* (IEEE, 2008), pp. 1–4.
[3]Z. B. Yan and J.-M. Liu, Ann. Phys. **358**, 206 (2015).
[4]H. Liu, Y. Wang, J. Wu, G. Zhang, and Y. Yan, Phys. Chem. Chem. Phys. **17**, 9098 (2015).
[5]S. Kundu, M. Clavel, P. Biswas, B. Chen, H.-C. Song, P. Kumar, N. N. Halder, M. K. Hudait, P. Banerji, M. Sanghadasa, and S. Priya, Sci. Rep. **5**, 12415 (2015).
[6]B.-O. Cho, T. Yasue, H. Yoon, M.-S. Lee, I.-S. Yeo, U.-I. Chung, J.-T. Moon, and B.-I. Ryu, in *2006 International Electron Devices Meeting* (IEEE, 2006), pp. 1–4.
[7]L. D. Bozano, B. W. Kean, V. R. Deline, J. R. Salem, and J. C. Scott, Appl. Phys. Lett. **84**, 607 (2004).
[8]G. Sassine, S. La Barbera, N. Najjari, M. Minvielle, C. Dubourdieu, and F. Alibart, J. Vac. Sci. Technol. B **34**, 012202 (2016).
[9]T. Su and H. Zhang, PLoS One **12**, e0171050 (2017).
[10]S. H. Jo, K.-H. Kim, and W. Lu, Nano Lett. **9**, 496 (2009).
[11]A. Kumar, M. Das, V. Garg, B. S. Sengar, M. T. Htay, S. Kumar, A. Kranti, and S. Mukherjee, Appl. Phys. Lett. **110**, 253509 (2017).
[12]J. Xiao, T. S. Herng, J. Ding, and K. Zeng, J. Alloys Compd. **709**, 535 (2017).
[13]S. Kim, H. Moon, D. Gupta, S. Yoo, and Y.-K. Choi, IEEE Trans. Electron Devices **56**, 696 (2009).
[14]L. Hu, J. Yuan, Y. Ren, Y. Wang, J.-Q. Yang, Y. Zhou, Y.-J. Zeng, S.-T. Han, and S. Ruan, Adv. Mater. **30**, 1801232 (2018).
[15]A. Ghosh, N. Kumari, and A. Bhattacharjee, Pramana **84**, 621 (2015).
[16]C.-C. Lin, Z.-L. Tseng, K.-Y. Lo, C.-Y. Huang, C.-S. Hong, S.-Y. Chu, C.-C. Chang, and C.-J. Wu, Appl. Phys. Lett. **101**, 203501 (2012).
[17]H. Yu, M. Kim, Y. Kim, J. Lee, K.-K. Kim, S.-J. Choi, and S. Cho, Electron. Mater. Lett. **10**, 321 (2014).
[18]F. M. Simanjuntak, O. K. Prasad, D. Panda, C.-A. Lin, T.-L. Tsai, K.-H. Wei, and T.-Y. Tseng, Appl. Phys. Lett. **108**, 183506 (2016).
[19]D. Xu, Y. Xiong, M. Tang, and B. Zeng, J. Alloys Compd. **584**, 269 (2014).
[20]H. Li, Q. Chen, X. Chen, Q. Mao, J. Xi, and Z. Ji, Thin Solid Films **537**, 279 (2013).
[21]M. H. Tang, Z. Q. Zeng, J. C. Li, Z. P. Wang, X. L. Xu, G. Y. Wang, L. B. Zhang, S. B. Yang, Y. G. Xiao, and B. Jiang, Solid State Electron. **63**, 100 (2011).
[22]A. Furukawa, N. Ogasawara, R. Yokozawa, and T. Tokunaga, Jpn. J. Appl. Phys. **47**, 8799 (2008).
[23]Q. Ma, D. B. Buchholz, and R. P. H. Chang, Phys. Rev. B **78**, 214429 (2008).
[24]M. C. Kim, K. Y. Lim, C. O. Kim, and S.-H. Choi, J. Korean Phys. Soc. **59**, 304 (2011).
[25]T. S. Herng, M. F. Wong, D. Qi, J. Yi, A. Kumar, A. Huang, F. C. Kartawidjaja, S. Smadici, P. Abbamonte, C. Sánchez-Hanke, S. Shannigrahi, J. M. Xue, J. Wang, Y. P. Feng, A. Rusydi, K. Zeng, and J. Ding, Adv. Mater. **23**, 1635 (2011).
[26]C. Wang, K. Jin, Z. Xu, L. Wang, C. Ge, H. Lu, H. Guo, M. He, and G. Yang, Appl. Phys. Lett. **98**, 192901 (2011).
[27]S. Kundu, D. Maurya, M. Clavel, Y. Zhou, N. N. Halder, M. K. Hudait, P. Banerji, and S. Priya, Sci. Rep. **5**, 8494 (2015).
[28]H. Tian, X. Wang, Y. Zhu, L. Liao, X. Wang, J. Wang, and W. Hu, Appl. Phys. Lett. **110**, 043505 (2017).
[29]J. Xiao, T. S. Herng, J. Ding, and K. Zeng, Acta Mater. **123**, 394 (2017).
[30]X. Luo, L. T. Tseng, W. T. Lee, T. T. Tan, N. N. Bao, R. Liu, J. Ding, S. Li, V. Lauter, and J. B. Yi, Sci. Rep. **7**, 6341 (2017).
[31]S. M. Jilani, T. D. Gamot, P. Banerji, and S. Chakraborty, Carbon **64**, 187 (2013).
[32]A. Sreedhar, J. H. Kwon, J. Yi, J. S. Kim, and J. S. Gwag, Mater. Sci. Semicond. Process. **49**, 8 (2016).
[33]S. Horzum, E. Torun, T. Serin, and F. M. Peeters, Philos. Mag. **96**, 1743 (2016).
[34]K. Milenova, I. Stambolova, V. Blaskov, A. Eliyas, S. Vassilev, and M. Shipochka, J. Chem. Technol. Metall. **48**, 259 (2013), available at https://www.scopus.com/record/display.uri?eid=2-s2.0-84884137653&origin=inward.
[35]A. Janotti and C. G. Van de Walle, Phys. Rev. B **76**, 165202 (2007).
[36]P. Biswas, S.-D. Baek, S. H. Lee, J.-W. Kim, J.-H. Park, S. J. Lee, T. Il Lee, and J.-M. Myoung, Appl. Phys. Lett. **109**, 171102 (2016).
[37]Y. Y. Tay, S. Li, C. Q. Sun, and P. Chen, Appl. Phys. Lett. **88**, 173118 (2006).
[38]S. U. Awan, S. K. Hasanain, M. F. Bertino, and G. H. Jaffari, J. Phys. Condens. Matter **25**, 156005 (2013).
[39]K.-S. Ahn, T. Deutsch, Y. Yan, C.-S. Jiang, C. L. Perkins, J. Turner, and M. Al-Jassim, J. Appl. Phys. **102**, 023517 (2007).
[40]S. Shraavan, S. Challagulla, S. Banerjee, and S. Roy, Bull. Mater. Sci. **40**, 1415 (2017).
[41]A. Z. Thong, M. S. P. Shaffer, and A. P. Horsfield, Sci. Rep. **8**, 9120 (2018).
[42]K.-W. C. Yang and S. J. T. Owen, IEEE Trans. Electron Devices **30**, 452 (1983).
[43]C. Chen, F. Pan, Z. S. Wang, J. Yang, and F. Zeng, J. Appl. Phys. **111**, 013702 (2012).
[44]A. Kumar, S. Mukherjee, and A. Kranti, J. Phys. D: Appl. Phys. **51**, 405601 (2018).
[45]Y. Huang, H. Lü, H. Guo, L. Liu, M. HE, Z. Chen, Y. Zhou, K. Zhao, K. Jin, and G. Yang, Chin. Sci. Bull. **51**, 2035 (2006).
[46]Y. Wu, L. Zhang, G. Xie, J.-L. Zhu, and Y. Chen, Appl. Phys. Lett. **92**, 012115 (2008).
[47]M. Karger and M. Schilling, Phys. Rev. B **71**, 075304 (2005).
[48]Z. Hong-Jian, Z. Xiao-Ping, and Z. Yong-Gang, Chin. Phys. Lett. **26**, 077303 (2009).
[49]C. Dubourdieu, J. Bruley, T. M. Arruda, A. Posadas, J. Jordan-Sweet, M. M. Frank, E. Cartier, D. J. Frank, S. V. Kalinin, A. A. Demkov, and V. Narayanan, Nat. Nanotechnol. **8**, 748 (2013).
[50]J. Xiao, W. L. Ong, Z. Guo, G. W. Ho, and K. Zeng, ACS Appl. Mater. Interfaces **7**, 11412 (2015).
[51]C. W. Zou, H. J. Wang, M. L. Yin, M. Li, C. S. Liu, L. P. Guo, D. J. Fu, and T. W. Kang, J. Cryst. Growth **312**, 906 (2010).
[52]W. L. Ong, H. Huang, J. Xiao, K. Zeng, and G. W. Ho, Nanoscale **6**, 1680 (2014).
[53]A. Q. Jiang, C. Wang, K. J. Jin, X. B. Liu, J. F. Scott, C. S. Hwang, T. A. Tang, H. Bin Lu, and G. Z. Yang, Adv. Mater. **23**, 1277 (2011).
[54]S. Farokhipoor and B. Noheda, APL Mater. **2**, 056102 (2014).
[55]T. L. Qu, Y. G. Zhao, D. Xie, J. P. Shi, Q. P. Chen, and T. L. Ren, Appl. Phys. Lett. **98**, 173507 (2011).
[56]J. Choi, J.-S. Kim, I. Hwang, S. Hong, I.-S. Byun, S.-W. Lee, S.-O. Kang, and B. H. Park, Appl. Phys. Lett. **96**, 262113 (2010).
[57]S. Hong, T. Choi, J. H. Jeon, Y. Kim, H. Lee, H.-Y. Joo, I. Hwang, J.-S. Kim, S.-O. Kang, S. V. Kalinin, and B. H. Park, Adv. Mater. **25**, 2339 (2013).
[58]S. V. Kalinin and D. A. Bonnell, J. Appl. Phys. **87**, 3950 (2000).